Nigerian Journal of Water Resources
2024, 10(1): 115-123
Print ISSN: 115-9944
Online ISSN: 2795-3793

ASSESSMENT OF GROUNDWATER POTENTIAL OF KATSINA, (SHEET 34) VIA THE INTERPRETATION OF SURFACE AND SUBSURFACE STRUCTURES USING AIRBORNE MAGNETIC AND PANCHROMATIC BAND 8 OF LANDSAT 8 DATA

[1]TAWEY, M.D (PHD), [2]MOHAMMAD, I., AND [3]IBRAHIM, A. A., ADEBAYO A.O. AMINU G.H, AND DOGARA S. B.

National Water Resources Institute, Mando Road Kaduna
Corresponding Author email: taweymam@gmail.com

ABSTRACT

This research was aimed to delineate the groundwater potential zone within Katsina and its environs using aeromagnetic and panchromatic band 8 of the Landsat 8 dataset via structural interpretation. To achieve the aim, the Centre for Exploration Targeting (CET) was applied to the residual magnetic intensity data of the study reduced to the equator (RTE) to delineate the subsurface structures. The Geomatica software helped extract the surface structures in the panchromatic band 8 of the Landsat 8 image. The surface and subsurface structures were merged to obtain the composite structural map of the study area. Line density analysis of the spatial analyst tool of ArcMap version 10.0.7 was applied to produce the total structural density map of the area that was subsequently classified into very-low, low, moderate, high and very-high groundwater potential zones. The work revealed that the very high groundwater potential zone covers 19,640.14 hectares and was estimated to be 6.54 % of the total study area with a structural density range of 1.40 km/km^2 to 1.75 km/km^2. The high groundwater potential zones have structural densities that range from 1.05 km/km^2 to 1.40 km/km^2 covering 55,561.78 hectares with an estimated 18.50 % of the total study area. The moderate groundwater potential zones have structural density ranging from 0.7 km/km^2 to 1.1.05 km/km^2 covering 81,834.02 hectares with an estimated 27.25 % of the total study area. The low groundwater potential zones range from 0.35 km/km^2 to 0.70 km/km^2 covering 78,719.77 hectares with an estimated 26.26 % of the total study area. Portions with very-low groundwater potential zones have structural densities that range from 0 km/km^2 to 0.35 km/km^2 covering 64,550.86 hectares with an estimated 21.50 % of the total study area. since structures are conduits for groundwater within the study area, boreholes drilled within the very high and high groundwater potential zones will be very productive. Also, the result of this study will be helpful in groundwater management decisions within the studied zone.

Keywords: *Groundwater potential, structure, borehole, structural interpretation and structural density*

1.0 INTRODUCTION

Groundwater, accounting for 97% of nonfrozen freshwater, sustains ecosystems, maintains river baseflow, and stabilises land in compressed soils. Aquifers play an important role as natural storage for groundwater and can also buffer impacts which results from long-term and short-term climatic variations (IGRAC, 2021; Margat & van der Gun, 2013). Groundwater is an important natural resource for human development, sustaining rural populations and contributing to 50% of the world's population that benefit from it. Groundwater is crucial for agriculture, contributing to 40% of the world's irrigated crop production and irrigating nearly 100 million hectares of arable land (IGRAC, 2021; Margat & van der Gun, 2013). One of the Sustainable Development Goals (SDGs) of the United Nations (UN) is GOAL 6: Clean Water and Sanitation (Ensure availability and sustainable management of water and sanitation for all). Groundwater is known to be safe for drinking and other uses (Margat & van der Gun, 2013), and the present study area is majorly occupied by basement rocks (Figure 1) which have geological structures such as faults, joints, fractures and folds. These Geological structures are vital to groundwater occurrence and

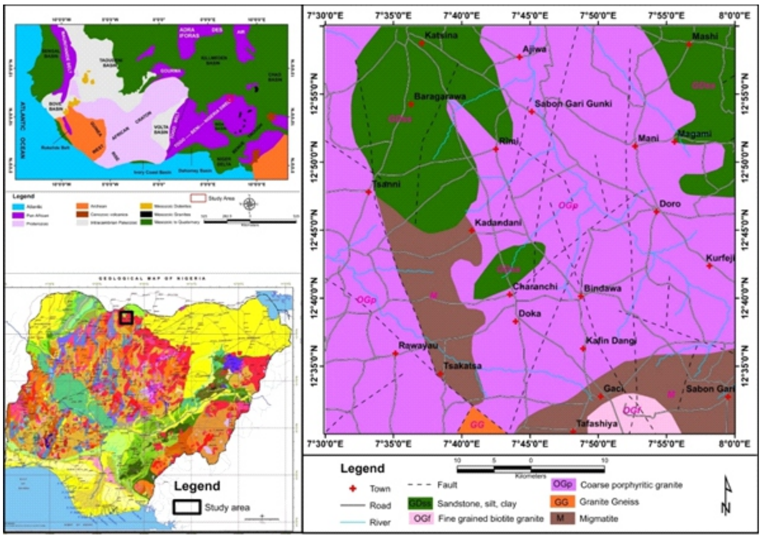

Figure 1: Location and Geologic Map of the Study Area (NGSA, 2009)

exploration (Ebele and Nur, 2020), as areas or portions with the intersection or cross junctions of these structures can hold and allow passage of large volumes of water (Nugroho and Tjahjaningsih, 2016; Gaafar, 2015 and 2012; Kassou *et al.,* 2012), and structures generally serve as a conduit for water flow within hard rocks.

Geological structural mapping is typically done through visual inspection of outcrops or geophysical resistivity fieldwork for groundwater exploration using an electrical resistivity meter. Available airborne magnetic and remote sensing data has made geological structural research easy, even in large area coverage areas. The magnetic technique is widely used and an accessible concept for identifying surface and subsurface geology and structures. (Eldosouky *et al.,* 2021; Gaafar, 2015).

Airborne magnetic data analysis aids in identifying and solving problems with local geologic mapping and structure (Eldosouky *et al.,* 2021, Eldosouky and Mohamed, 2020; Gaafar, 2015). Researchers are now integrating high-resolution remote sensing data with magnetic data for structural mapping purposes, and it is freely available for free download (Saibi *et al.,* 2016; Saadi *et al*., 2008). Since structures are conduits for groundwater movement and accumulation, portions with high structural density can point to a probable portion of groundwater accumulation and subsequent exploration. This is the motivation for this study.

This research is aimed at delineating the groundwater potential zone within Katsina and its environs using aeromagnetic and panchromatic band 8 of the Landsat 8 dataset via structural interpretation.

1.1 Location and Geology

The study area is situated in the northern part of Katsina state in northwestern Nigeria (Figure 1). It is bounded by Latitude 12°30'N to Latitude 13°00'N and Longitude 7°30'E to Longitude 8°00'E with an estimated total surface area of 3, 025 km^2. Katsina state's geology consists of basement and partially sedimentary basin rocks from the Iullemeden basin, also known as the Sokoto basin in Nigeria. The Migmatite-Gneiss Complex, a common component of Nigeria's basement complex, comprises diverse migmatites, orthogneisses, paragneisses, and metamorphosed rocks. Petrographic evidence suggests that Pan-African reshaping caused partial melting and recrystallisation, with most types exhibiting metamorphism (Rahaman, 1988; Dada, 2006). The Migmatite-Gneiss Complex spans the Pan-African to Eburnean ages (Obaje, 2009). Rock assemblages within the study area are fine-grained biotite granite, Migmatite, granite gneiss Porphyritic granite and sedimentary rock, siltstone, silt and clay (Figure 1), (NGSA, 2009).

2.0 Materials and Methods

2.1 Source of Remote Sensing Data

The remote sensing data used for this work is the panchromatic band 8 of Landsat 8 (OLI) which was downloaded from the United States Geological Survey (USGS) website (*https://earthexplorer.usgs.gov/*).

2.2 Source of aeromagnetic data

High-Resolution Aeromagnetic Data (HRAD) of part of Katsina state was acquired from the Nigeria Geological Survey Agency (NGSA). The data was acquired in 2009 by the NGSA.

2.3 Methods

The steps applied in this study include,

2.3.1 Magnetic Data Approach:

i. Application of the upward continuation filter attenuates shallow features and enhances deeper sources, making it suitable for regional-residual separation (Reynolds, 1997, Telford *et al.,* 1990) and has been applied in this study.

The equation (1) of the wavenumber domain filter to produce upward continuation is

$$F(\omega) = e^{-h\omega} \quad (1)$$

Where h is the continuation height. This function decays steadily with increasing wavenumber, attenuating the higher wavenumbers more severely, thus producing a map in which the more regional features predominate.

ii. Reduction to the Equator (RTE)

The RTE filter converts inclined data from vertical to horizontal, focusing anomalies at low magnetic latitudes, allowing for interpretation without compromising geophysical significance. The equation (2) which is used for RTE transformation is shown below.

$$L(\theta) = \frac{[\sin(I) - i.\cos(I).\cos(D-\theta)]^2 X(-\cos^2(D-\theta))}{[Sin^2(I_a) + Cos^2(I_a).Cos^2(D-\theta)]X[Sin^2(I) + Cos^2(I).Cos^2(D-\theta)]} \text{ if } (\backslash I_a \backslash) < (\backslash I \backslash), I_a = 1 \quad (2)$$

Where, *I* represent the geomagnetic inclination, is the inclination for amplitude correction; *D* represents the geomagnetic declination, Sin (*I*) is the amplitude component; while $i\cos(I)\cos(D-\theta)$ is the phase component.

Centre for Exploration Targeting (CET) for structural delineation

The CET algorithm suite enhances, detects, and analyses complex structures in field data, identifying promising ore deposits and lineaments using total magnetic intensity data (Core et al., 2009). The CET grid method enhances magnetic data by identifying discontinuity zones, intensity irregularities, and texture zones in restricted magnetic responses, often due to rock edges, elongated structures, and intrusions (Kovesi 1991). These zones are expressed as skeletal structures, with output data showing deviations and offsets within the structural characteristics (Kovesi, 1997).

2.3.2 Remote Sensing Data

The PCI Geomatica edge detection algorithm was applied to the panchromatic band 8 of the Landsat 8 image. Thresholding and filtering processes were done on the image after which, structural lineaments were extracted from the edges of the image by subjecting it to the line algorithm of PCI Geomatica.

3.0 RESULT AND DISCUSSION

3.1 Residual Magnetic Intensity (RMI) Map

Figure 2a shows a colour-shaded map of the study's residual magnetic intensity, varying from -77.3 nT low to 120.5 nT high, based on different rock types. Low magnetic intensity areas are in deep blue, while high magnetic intensity is shown in red to pink. The low observed around Katsina and Mashi due to deeper magnetic sources and sedimentary rocks. Between Kankiya and Bindawa, there is an observed occurrence of magnetic low and magnetic high in an alternating manner, this can also be attributed to the presence of subsurface geological structures. Figure 2b shows a colour-shaded map of residual magnetic intensity reduced to the equator in the study area, varying from -76.1 nT low to 100.6 nT high. Low areas have deep blue

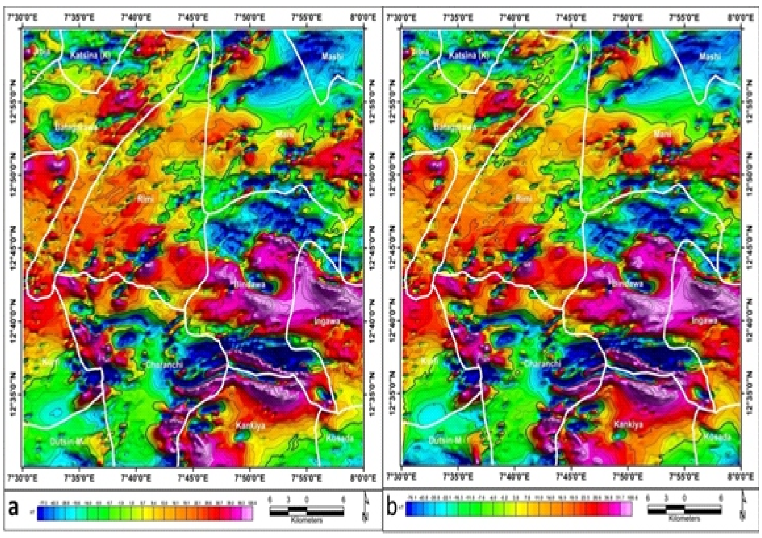

Figure 2: a. RMI map and b. RTE map

colouration, while high areas have red to pink. The alternating pattern in magnetic low and high is observed between Kankiya and Bindawa and is attributed to subsurface geologic structures.

Comparing the two maps (Figures 2a and 2b) reveals changes in anomaly amplitudes. The RMI and RTE maps showed differences in legend and amplitude variation in the southwestern and southern parts of Dutsin-ma, and in the northern part from west to east. The central portion of the maps also exhibited variations in anomaly amplitudes.

3.2 Subsurface Structures from the CET

Figure 3a is the study area's subsurface structural map, delineated using CET data and overlayed on the RTE map, and it confirms the presence of subsurface geological structures in Figure 3b, such as those between Kankiya and Bindawa, Charanchi and Kankiya, Kurfi and Charanchi. The structural map (Figure 3b) reveals faulted or fractured portions between Kankiya, Charanchi,

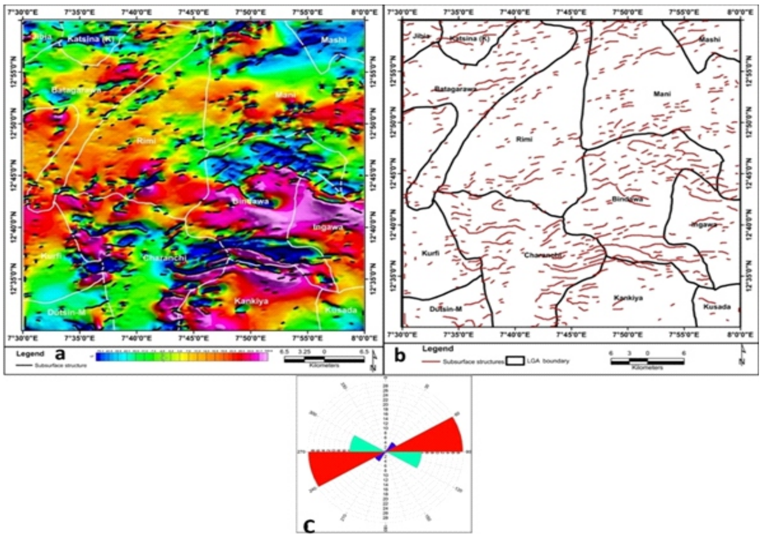

Figure 3: a. Subsurface CET structures on the RTE map, b. the CET Structural Map and c. Rose diagram

and Bindawa, with trends NW-SE, NE-SW, and EW revealing the structure's clearer visibility. Portions between Charanchi, Kurfi, and Rimi are also highly faulted and jointed (Figure 3b). The areas with numerous faults are suitable for groundwater exploitation as they serve as the host and conduit for groundwater movement. Subsurface structural trend analysis using the Rose diagram (Figure 3c) revealed that the most predominant subsurface structural trend within the study area is the east-northeast to west-south-west (ENE-WSW) followed by west-northwest to east-south-east (WNW-ENE) and lastly northeast to southwest (NE-SW).

3.3 Surface Structures from Landsat 8

Figure 4a shows panchromatic band 8 of the Landsat 8 data map, while Figure 4b shows surface structures from the analysis of band 8 of Landsat 8 data. PCI Geomatica's edge detection algorithm was applied to the band-8 data, extracting surface structural lineaments. On this map (Figure 4a), surface structures were observed to be evenly distributed, except for Mani Local Government Area, which has sparse distribution.

The surface structural rose diagram (Figure 4c) reveals a predominant east-north-east to west-south-west (ENE-WSW) trend, followed by northeast-to-southwest (NE-SW), north-north-east to south-south-west (NNE-SSW), WNW-ENE, NWN-SSE, and NW-SE.

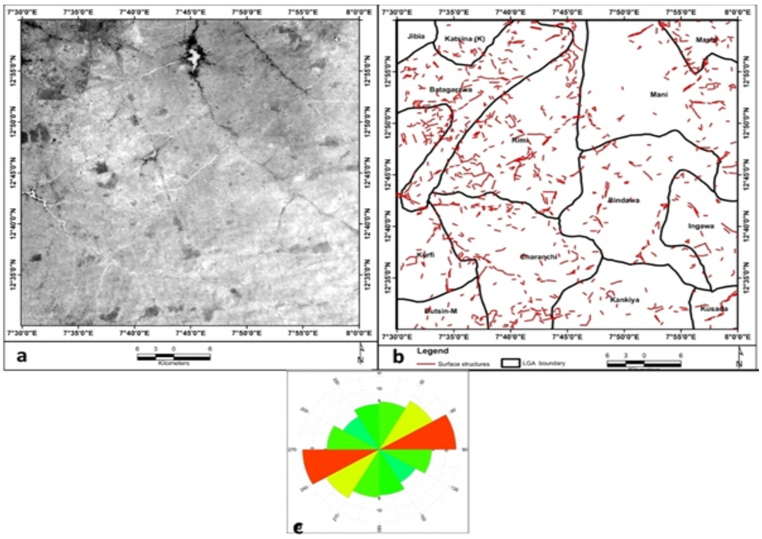

Figure 4: a. band 8 of Landsat 8,
b. Surface structures and b. Rose diagram

3.4 Structural Density and Groundwater Potential Zone (GWPZ) Interpretation

The combined surface and subsurface structural map of the study area is represented by Figure 5, with Figure 6 representing the combined structural density map of the area showcasing possible portions of very-low, low, moderate, high and very-high GWPZs.

Geological structures significantly impact groundwater circulation, with fracture zones and joint intersections often being the optimal locations for groundwater accumulation within hard rocks (Caponella,1989). Therefore, areas with the highest structural density

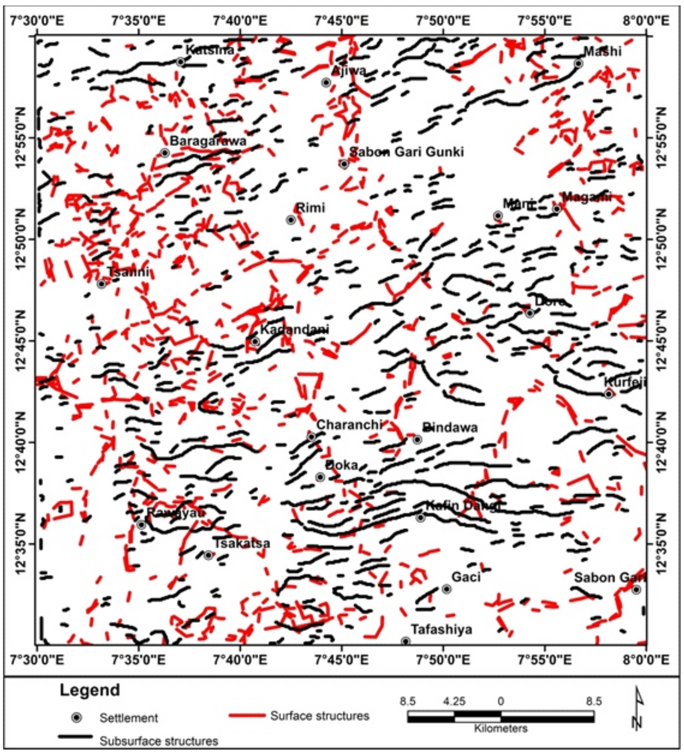

Figure 5: Combined Structural Map of the Area

(1.40 - 1.75 km/km^2), are portions having very high groundwater potentials covering 19,640.14 hectares as displayed in Table 1, with an estimated 6.54 % of the total study area.

The high GWPZ based on the structural density analysis have revealed the structural density of this environment to range from 1.05 km/km^2 to 1.40 km/km^2 having high groundwater potentials covering 55,561.78 Hectares with an estimated 18.50 % of the total study area. The moderate GWPZ based on the structural density analysis have revealed the structural density of this environment to range from 0.7 km/km^2 to 1.1.05 km/km^2 having moderate groundwater potentials covering 81,834.02 hectares with an estimated 27.25 % of the total study area.

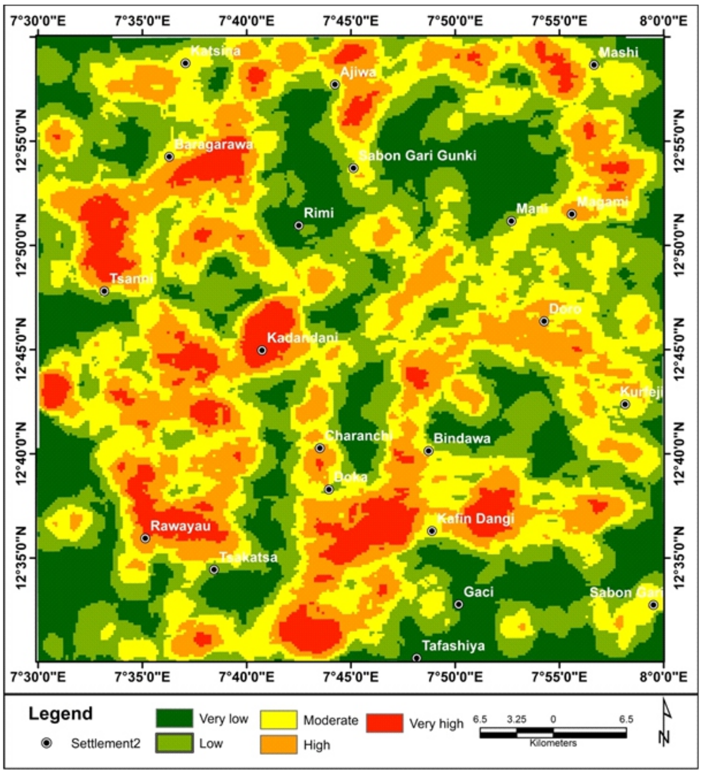

Figure 5: Groundwater Potential Zones (GWPZ) Map of the Area

Table 1. Showing structural densities, area coverage and percentages of groundwater potential zones

S/N	Structural Density (km/km^2)	Type	Area (Hecter)	Percentage
1	0 - 0.35	Very low	64,550.66016	21.50
2	0.35 - 0.70	Low	78,719.77344	26.21
3	0.70 - 1.05	Moderate	81,834.01563	27.25
4	1.05 - 1.40	High	55,561.78125	18.50
5	1.40 - 1.75	Very High	19,640.13672	6.54

The low GWPZ based on the structural density analysis has revealed the structural density of this area ranging from 0.35 km/km^2 to 0.70 km/km^2 having high groundwater potentials covering 78,719.77 hectares with an estimated 26.26 % of the total study area. Portions with very-low GWPZ based on the structural density analysis have revealed the structural density of this environment ranges from 0 km/km^2 to 0.35 km/km^2 having high GWPZ that cover 64,550.86 hectares with an estimated 21.50 % of the total study area.

4.0 Conclusion

The delineated structures have aided in the production of the structure density map of the study area and subsequently classified into very-low, low, moderate, high and very-high groundwater potential zones. Boreholes drilled within very high and high groundwater potential zones will be very productive. The result of this study will be helpful in groundwater management as the need arises.

REFERENCES

Caponella, F. (1989). Remote sensing image interpretation for Groundwater Surveying in Remote sensing /Application for Water Resources. Report of the 13th UN/FAD/UNESCO International Training Course; RSC-Series, 50 -292.

Core, D., Buckingham, A., & Belfield, S. (2009). Detailed structural analysis of magnetic data done quickly and objectively. *Specialist group in economic geology (SGEG) Newsletter*. (April).

Dada, S. S. (2006). Proterozoic evolution of Nigeria. In: Oshi O (Ed.), The basement complex of Nigeria and its mineral resources (A Tribute to Prof. M. A. O. Rahaman). Akin Jinad and Co. Ibadan, 29-44.

Ebele, J. E., & Nur, A. (2020). Regional groundwater studies using high-resolution aeromagnetic data in Abuja and environs, North-Central Nigeria. Applied Journal of Physical Science, 2(3), 68-79.

Eldosouky, A. M., Elkhateeb, S. O., Mahdy, A. M., Saad, A. A., Fnais, M. S., Abdelrahman, K., & Andráš, P. (2021). Structural analysis and basement topography of Gabal Shilman area, Southeastern Desert of Egypt, using aeromagnetic data. Journal of King Saud University-Science. https://doi.org/10.1016/j.jksus.2021.101764

Eldosouky, A.M., Mohamed, H., 2021. Edge detection of aeromagnetic data as effective tools for structural imaging at Shilman area, South Eastern Desert. Egypt. *Arabian Journal of Geosciences* 14, 13. https://doi.org/10.1007/s12517-020-06251-4.

Gaafar, I. (2015) Integration of geophysical and geological data for delimitation of mineralised zones in Um Naggat area, central eastern desert, Egypt. *NRIAG Journal of Astronomy and Geophysics.* 4, 86-99

Ge, T., Qiu, L., He, J., Fan, Z., Huang, X., Xiong, S., 2020. Aeromagnetic identification and modelling of mafic-ultramafic complexes in the Huangshan-Turaergen Ni-Cu metallogenic belt in NW China: Magmatic and metallogenic implications. Ore Geol. Rev. 127. https://doi.org/10.1016/j.oregeorev.2020.103849 103849.

IGRAC (International Groundwater Resources Assessment Centre), 2021. Transboundary Aquifers of the World [map]. Edition 2021. Scale 1: 50 000 000. Delft, Netherlands: IGRAC, 2021

Kassou, A., Essahlaoui, A., and Aissa, M (2012) Extraction of Structural Lineaments from Satellite Images Landsat 7 ETM+ of Tighza Mining District (Central Morocco) *Research Journal of Earth Sciences* 4 (2): 44-48, 2012 ISSN 1995-9044 © IDOSI Publications, 2012 DOI: 10.5829/idosi.rjes.2012.4.2.1110

Kovesi, P. (1991). Image features from phase congruency”, *Videre: Journal of Computer Vision Research*, *Summer*. The MIT Press,1(3), 2-27.

Kovesi, P. (1997): Symmetry and asymmetry from local phase, AI '97, Tenth Australian. *Joint Conference on Artificial Intelligence*, 2-4.

Margat, J., & van der Gun, J. (2013). Groundwater around the world: a geographic synopsis. Leiden, Netherlands: CRC Press/Balkema

NGSA, (2009). Geology and structural lineament map of Nigeria.

Nugroho, U. C., & Tjahjaningsih, A. (2016). Lineament Density Information Extraction Using Dem SRTM Data to Predict the Mineral Potential Zones. *International Journal of Remote Sensing and Earth Sciences*, 13(1), 67-74.

Obaje, N. G. (2009). *Geology and Mineral Resources of Nigeria*, Berlin: Springer-Verlag, Heidelberg. 35-48.

Obi, D. A, Ilozobhie, A. J., and Abua, J. U. (2015) Interpretation of aeromagnetic data over the Bida Basin, North Central, Nigeria

Rahaman MA, Ocan O (1978) On relationships in the Precambrian Migmatite-gneisses of Nigeria. Niger J Min Geol 15:23–32

Rahaman MA (1988) Recent advances in the study of the basement complex of Nigeria. In: Geological Survey of Nigeria (ed) Precambrian Geol Nigeria, pp 11-43

Reynolds, J. M. (1997). *An introduction to applied and environmental geophysics*, John Wiley & Ltd. Bans Lane, Chichester.124-132.

Saadi, N. M., Watanabe, K., Imai, A., and Saibi, H. (2008) Integrating potential fields with remote sensing data for geological investigations in the Eljufra area of Libya. *Earth Planets Space*, 60, 539-547

Saibi, H., Masood Azizi, M., and Mogren, S. (2016) Structural Investigations of Afghanistan Deduced from Remote Sensing and Potential Field Data. *Acta Geophysica*. 64 (4), 978-1003 DOI: 10.1515/acgeo-2016-0046

Sanusi, S. O and Amigun, J. O. (2020). Structural and hydrothermal alteration mapping related to orogenic gold mineralization in part of Kushaka schist belt, North-central Nigeria, using airborne magnetic and gamma-ray spectrometry data.

Telford, W. M., Geldart, L.P., Sherriff, R. E., & Keys, D. A. (1990). *Applied geophysics.* Cambridge: Cambridge University Press, 86